EUROPEAN ORGANIZATION FOR NUCLEAR RESEARCH

CERN-EP/84-141
22 October 1984

PROPERTIES OF AN OPTICAL PHASE-SHIFTER MADE OF TWO GOLD MIRRORS

S. Carusotto[1], E. Iacopini[1], E. Polacco[1],
F. Scuri[2], G. Stefanini[2] and E. Zavattini[2]

ABSTRACT

Reflectivity and phase-shift properties of a device composed of two flat mirrors with a gold coating 1 μm thick have been measured, at some relevant light incidence angles, for λ_1 = 488 nm and λ_2 = 514.5 nm. An experimental investigation of the low-frequency noise (around 50 mHz) contributed by the phase-shifter in an ellipsometer is described.

(Submitted to Applied Physics B)

1) Dipartimento di Fisica, Pisa, Italy and INFN, Sez. Pisa, Italy.
2) CERN, Geneva, Switzerland.

1. INTRODUCTION

Properties of light reflection on absorbing-media surfaces have been extensively studied in ellipsometry [1]-[5], and the ellipsometric parameters have been measured in the optical analysis of thin metallic films [6], [7].

Reflection on metallic surfaces has been used to measure the magnetic birefringence of noble gases [8] with two metallic mirrors acting as a 90° phase-shifter, and the ellipsometer reached a sensitivity of $3.6 \cdot 10^{-8}/\sqrt{\text{Hz}}$ when the signal frequency was around 2 Hz.

Ellipsometric techniques can be applied to the study of the photon-photon interaction in the visible region [9], [10]. According to the proposed method, it is necessary to measure the very small ellipticity induced on a linearly polarized light beam traversing a vacuum region where a very high modulated transverse magnetic field B ($|B| \approx 80$ kG) is present; it is expected that for such high value of the field B the modulation frequency cannot exceed a few tens of milliherz.

For this purpose we are developing at CERN a high-sensitivity ellipsometer based on a 90° phase-shifter. We have found that a quarter-wave plate, in addition to its poor tunability, gives too much ellipticity noise below 100 mHz to let our ellipsometer reach a sufficiently good sensitivity. Furthermore, the quarter-wave plate is sensitive to stray magnetic fields. For these reasons we have investigated the tunability, the stability in phase-shift, and the noise introduced at the frequencies below 1 Hz by a device composed of two parallel gold-coated mirrors.

The phase shift Δ_t introduced by the device between the two light components linearly polarized parallel to the incidence plane and orthogonal to it, is a function of the incidence angle θ and of the wavelength λ. We call 'principal angles' the incidence angles $\bar{\theta}$ for which $\cos\Delta_t = 0$, i. e. when the device acts as a perfect $\lambda/4$ retarder.[1]

In Section 2 we describe a method and a set-up for measuring the phase shift Δ_t within 1 mrad. As a check, we have measured the refractive index of the two gold coatings.

In Section 3 we present our results. In Section 4 we discuss the low-frequency noise of the system and we find a sensitivity of $1.7 \cdot 10^{-8}$ $\sqrt{\text{Hz}}$ at 56 mHz of signal frequency.

2. METHOD AND EXPERIMENTAL SET-UP

The set-up used to measure the phase-shift Δ_t due to the device M as a function of the incidence angle θ is shown in fig. 1. The light source is a CW argon-ion laser (Lexel, mod. 295), tuned at $\lambda_1 = 488$ nm or $\lambda_2 = 514.5$ nm for an output power of about 300 mW. The polarization plane after the Glan-Thompson polarizer prism P (Karl Lambrecht) is parallel or orthogonal to the incidence plane. The air Faraday cell FCA1 introduces a rotation of the light polarization plane modulated at frequency f_{a1} with a peak amplitude Φ_{a1}. The device M is composed of two mirrors obtained by

---

[1] For a system of two parallel metallic mirrors one has m principal angles $\bar{\theta}_m$ for which $\Delta_t = +90^\circ$, and m for which $\Delta_t = -90^\circ$ if m is the number of reflections on each surface.

evaporating 1 μm of gold on BK7 optical flats. The two mirrors are mounted parallel to each other at a distance of ≈ 1 cm on the same goniometer plate turning in the optical bench plane.

After M, a second air Faraday cell FCA2 and the glass Faraday cell FCG introduce plane polarization rotations modulated at the frequencies f_{a2} and f_g, with peak amplitudes $\Phi_{a2} = \Phi_{a1}$ and Φ_g, respectively. The characteristics of the cells FCA1, FCA2, and FCG are specified in table 1.

An heterodyne method is employed where the cell FCG acts as a carrier for the small rotation signals due to the air cells FCA1 and FCA2. The features of the cell FCG are chosen in order to be optimized with respect to the requested rotation value, and to the noise in the light polarization state introduced by the glass. A 9 mm thick BK7 optical flat (mounted in a cylindrical plastic container mechanically isolated from the coil) has been found adequate for working with a light power of I ≈ 100 mW on the cell. The power dissipation on the water-cooled solenoid is ≈ 4 W for the modulation peak value. The signal for the FCG cell, as for the other cells FCA1 and FCA2, is derived from frequency synthetizers (HP 3325A).

The light coming out of the cell FCG is analysed by the prism A crossed for extinction. The intensity transmitted by the analyser prism A, for light linearly polarized prism P parallel to the incidence plane of M, is given by the following expression (to first order in Φ_{a1} and Φ_{a2}):

$$I(t) \approx I_0[\sigma^2 + \Phi_g^2\cos^2(2\pi f_g t)$$

$$+ (\alpha + (R_s/R_p)\beta\sin\Delta_t)\Phi_g\cos(2\pi f_g t)$$

$$+ 2(R_s/R_p)\Phi_g\Phi_{a1}\cos\Delta_t\cos(2\pi f_g t)\cos(2\pi f_{a1} t)$$

$$+ 2\Phi_g\Phi_{a2}\cos(2\pi f_g t)\cos(2\pi f_{a2} t)], \qquad (1)$$

where I_0 is the light intensity before A; σ^2 is the over-all extinction factor ($\sigma^2 \approx 5 \cdot 10^{-8}$); α is the unavoidable optical misalignment; β is the uncompensated residual ellipticity before the mirrors (α and $\beta < 10^{-4}$ rad); R_p, R_s, and Δ_t are defined by the following equations:

$$R_p = |\rho_p|^{2m}, \quad R_s = |\rho_s|^{2m}, \qquad (2)$$

$$\Delta_t = 2m\Delta, \qquad (3)$$

where ρ_p and ρ_s are the complex ratios between the reflected and the incident wave amplitudes of each gold coating for light linearly polarized in the incidence plane and in the orthogonal direction, respectively, m is the number of reflections per surface, and Δ is the phase-difference between ρ_s and ρ_p.

Since $\Phi_{a1} = \Phi_{a2}$, the ratio Q between the last two terms of eq. (1) is given by

$$Q = (R_s/R_p)\cos\Delta_t. \qquad (4)$$

Therefore the principal angles are determined by measuring the ratio Q as a function of the incidence angle θ. For the case in which the polarization plane after the prism P is orthogonal to the incidence plane, the quantities R_s and R_p must be interchanged in eqs. (1) and (4).

The light intensity I(t) is detected by the PIN photodiode D (see fig. 1), and the voltage signal coming from the preamplifier of D is first demodulated by the phase-sensitive detector PSD (E & EG Brookdeal Ortholoc SC 9095) locked at the frequency f_r, with $f_r = f_g$, and then processed by a low-frequency spectrum analyser (HP 3582A).

Typical spectra of the PSD output in the frequency region of the FCA1 and FCA2 signals are shown in fig. 2. The peak amplitudes at the frequencies f_{a1} and f_{a2} are proportional to the last two terms of eq. (1), respectively. A series of spectra were taken in order to find the principal angles.

To check our results we have also measured the complex refractive index n^* of each gold mirror with the set-up shown in fig. 3.

The method is based on well-known ellipsometry techniques [1], [3], [5], [6]. The light source is still the CW argon-ion laser; in this case the light is linearly polarized at 45° with respect to the plane of incidence. The gold mirror MG is mounted on a goniometer plate RP rotating on the bench plane; the PIN photodiode D measures the transmitted light intensity at four particular angles δ between the polarization plane of the prism P and the prism A. The voltage signal from the photodiode amplifier is given by

$$V(\delta=0^0) = \eta[(|\rho_p|^2+|\rho_s|^2) + 2|\rho_p||\rho_s|\cos\Delta]I_0/4, \quad (5)$$

$$V(\delta=45^0) = \eta|\rho_p|^2 I_0/2, \quad (6)$$

$$V(\delta=90^0) = \eta[(|\rho_p|^2+|\rho_s|^2) - 2|\rho_p||\rho_s|\cos\Delta]I_0/4, \quad (7)$$

$$V(\delta=135^0) = \eta|\rho_s|^2 I_0/2, \quad (8)$$

where I_0 is the light intensity before the gold mirror and η is a suitable constant.

From the measured quantities (5) to (8), we obtain the following ratios:

$$V(\delta=135^0)/V(\delta=45^0) = |\rho_s|^2/|\rho_p|^2, \quad (9)$$

$$[V(\delta=0^0) - V(\delta=90^0)]/2\sqrt{V(\delta=45^0)V(\delta=135^0)} = \cos\Delta, \quad (10)$$

from which the real part n and the imaginary part k of n^* can be easily deduced ($n^* = n + ik$) as shown in ref.[11] [eqs. (26a) and (26b), chapter 13.2].

3. ELLIPSOMETRIC PARAMETERS

Tables 2-5 list the values of n and k obtained using the apparatus of fig. 3 for incidence angles θ around the values θ' and θ'' for which $\Delta = 45^0$ and $\Delta = 135^0$, respectively. For each mirror the average values $\langle n \rangle$ and $\langle k \rangle$ of the real and complex part of the refractive index have been obtained at the wavelengths λ_1 and λ_2; the quoted systematic error is mainly due to the

uncertainty of the absolute value of the incidence angle. The results for the two mirrors agree within the errors; for computer calculations (see below) we have assumed the following values of n and k averaged over all measured incidence angles for both mirrors:

$$n = 1.024, \quad k = 1.541 \quad \text{at} \quad \lambda_1 = 488 \text{ nm}, \tag{11}$$

$$n = 0.599, \quad k = 1.705 \quad \text{at} \quad \lambda_2 = 514.5 \text{ nm}. \tag{12}$$

It is difficult to compare values (11) and (12) with those reported in refs. [6], [12], and [13], since these latter have been measured at different wavelengths and for gold thickness below 0.1 μm.

Figure 4 shows the phase difference Δ and the ratio $\tan\Psi = |\rho_s|/|\rho_p|$ obtained from eqs. (9) and (10); the dashed lines give the values of Δ and $\tan\Psi$ as calculated using the average values (11) and (12) of the refractive index. In the same way we obtained the curves of $|\rho_s|$ and $|\rho_p|$ versus the incidence angle θ given in fig. 5.

With regard to the phase-shifting properties of the device M, the experimental values of the ratio Q, using the set-up of fig. 1 for a configuration of two reflections at $\lambda_2 = 514.5$ nm, are presented in figs. 6 and 7; they appear to be well fitted by the curve (dashed line), obtained by computer calculations, from the measured refractive index of the mirrors given in eqs. (11) and (12). Figure 8 shows the ratio Q for a configuration of three reflections per mirror around three of the principal angles.

From curves of figs. 6 and 7 it can be deduced that the principal angles for the configuration of two reflections are $\bar{\theta}_1 = 47.75^0$ and $\bar{\theta}_2 = 78.25^0$ at $\lambda_2 = 514.5$ nm. The accuracy for recovering the principal angles is $\delta\theta \approx \pm 0.5$ mrad, which corresponds to a spread in the phase shift $\delta\Delta_t \approx \pm 1$ mrad.

For $\theta = \bar{\theta}_1$ and $\theta = \bar{\theta}_2$ the FCA1 peak was completely plunged in the noise, which gives a limit for the Q ratio of about -52 dB.

After one month, measurements were repeated at different laser powers in the range 0.1 to 0.3 W; we found no changes within the error.

4. LOW-FREQUENCY NOISE PROPERTIES

In order to study the low-frequency noise introduced by the phase-shifter M in the set-up of fig. 1, we have done a series of runs with M for the configuration of two reflections and $\bar{\theta}_2 = 78.25^0$; moreover, the light ($\lambda_2 = 514.5$ nm) was linearly polarized in the incidence plane. The modulation frequency of the cells FCA1 and FCA2 were $f_{a1} = 72$ mHz and $f_{a2} = 56$ mHz, respectively. The phase-sensitive detector PSD was locked at $f_r = 1600.8$ Hz so as to shift the peaks of the modulated signals from the zero frequency noise region.

We found that, in order to minimize the noise, special care had to be taken to ensure thermal stability of the elements P, M, FCG, and A. In particular, after alignment of the set-up before data-taking, it was necessary to wait a few hours for the optical parts to stabilize; moreover, any air drift had to be carefully avoided.

The measurements were done by analysing the PSD outputs with the spectrum analyser in the region 0 to 1 Hz. A typical spectrum is shown in fig. 9a, where the FCA1 signals which should appear at the frequencies 128 mHz and 272 mHz are extinguished because the phase-shifter M is placed at the principal angle $\overline{\theta_2}$.

We found that the sensitivity ξ, defined as the signal for which the signal-to-noise ratio is SNR = 1, depends on the signal frequency. In the optimum conditions of thermal stability, we have

$$\xi_0 = 1.7 \cdot 10^{-8}/\sqrt{\text{Hz}} \tag{13}$$

around 50 mHz. From 50 mHz down to 10 mHz, ξ increases, whereas in the region 0.5 to 1 Hz ξ decreases to about $\xi_0/2$.

We have also done some measurements with the M device removed; in this case we did not observe any increase of the noise in the region from 50 mHz downward (see fig. 9b). The noise level in this case was mainly due to the thermal fluctuations in the glass of the FCG cell; the noise contribution of the amplitude fluctuations in the synthetizer and in the amplifier driving the FCG was measured and found to be negligible. The laser intensity noise contribution accounts for less than $\xi_0/2$, given the excellent extinction factor of the set-up ($\sigma^2 \approx 5 \cdot 10^{-8}$) [10], [14].

ACKNOWLEDGEMENTS

We thank Messrs. B. Beck, R. Grabit, F. Jeanmairet, and B. Smith for their skilled technical support.

References

[1] W. Swindell, Appl. Opt. 7 (5), 943-49 (1968).

[2] D.E. Aspnes, J. Opt. Soc. Am. 64 (5), 639-46 (1974).

[3] D.E. Aspnes and A.A. Studna, Appl. Opt. 14 (1), 220-28 (1975).

[4] D. Chandler-Horowitz and G.A. Candela, Appl. Opt. 21 (16), 2972-77 (1982).

[5] A.I. Pen'kovskii, Sov. J. Opt. Technol. 49 (8), 510-13 (1982).

[6] P.H. Lissberger, I.W. Salter, M. Fitzpatrick and P.L. Taylor, J. Phys. E 10, 635-41 (1977).

[7] I. Ohlidal and F. Lukes, Thin Solid Film 85, 181-90 (1981).

[8] S. Carusotto, E. Iacopini, E. Polacco, F. Scuri, G. Stefanini and E. Zavattini, J. Opt. Soc. Am. B 1 (4), 635-40 (1984).

[9] E. Iacopini and E. Zavattini, Phys. Lett. B 85 (1), 151-54 (1979).

[10] E. Iacopini, B. Smith, G. Stefanini and E. Zavattini, Nuovo Cimento 61B (1), 21-37 (1981).

[11] M. Born and E. Wolf, Principles of Optics, 6th ed. (Pergamon Press, Inc., New York, 1983).

[12] Landolt-Bornstein, Zahlenwerte und Funktionen, II. band, 8. teil, 1-12 (Springer-Verlag, Berlin, 1962).

[13] W.J. Anderson and W.N. Hansen, J. Opt. Soc. Am. 67 (8), 1051-58 (1977).

[14] J.H. Cole, Appl. Opt. 19 (7), 1023-25 (1980).

Table 1: Characteristics of the Faraday cells

Cell	Medium	Modulation frequency (Hz)	Peak excitation current (A)	Rotation charact. (rad/A)	Peak rotation amplitude (rad)
FCA1	air	3.6	0.2	$4.9 \cdot 10^{-6}$	$9.8 \cdot 10^{-7}$
FCA2	air	4.0	0.2	$4.9 \cdot 10^{-6}$	$9.8 \cdot 10^{-7}$
FCG	glass	1600.6	2.0	$2.7 \cdot 10^{-4}$	$5.4 \cdot 10^{-4}$

Table 2: Refractive index at λ_2 = 488 nm and $44^\circ < \theta < 54^\circ$; $\tan\Psi = |\rho_s|/|\rho_p|$.

	Mirror A				Mirror B			
θ (deg.)	tanΨ	|cosΔ|	n	k	tanΨ	|cosΔ|	k	n
44	1.38	0.815	0.986	1.520	1.39	0.843	1.112	1.583
45	1.41	0.819	1.107	1.593	1.40	0.830	1.112	1.605
46	1.41	0.790	1.034	1.573	1.42	0.784	1.007	1.537
47	1.44	0.779	1.084	1.592	1.42	0.752	0.966	1.527
48	1.45	0.741	1.030	1.564	1.47	0.759	1.092	1.572
49	1.47	0.715	1.037	1.560	1.46	0.700	0.967	1.522
50	1.49	0.702	1.066	1.593	1.50	0.712	1.089	1.593
51	1.50	0.666	1.037	1.584	1.50	0.662	1.020	1.560
52	1.51	0.637	1.030	1.598	1.55	0.665	1.130	1.601
53	1.53	0.595	1.016	1.568	1.55	0.599	1.042	1.551
54	1.56	0.568	1.049	1.577	1.56	0.574	1.059	1.580
Mean			1.043	1.574			1.054	1.566
St. dev.			0.033	0.022			0.058	0.029

Mean of both mirrors: $n' = 1.047$ $k' = 1.570$

Statistical error: $\sigma_n = 0.029$ $\sigma_k = 0.018$

Systematic error: $s_n = 0.010$ $s_k = 0.020$

Table 3: Refractive index at λ_2 = 488 nm and $73^\circ < \theta < 82^\circ$; $\tan\Psi = |\rho_s|/|\rho_p|$.

	Mirror A				Mirror B			
θ (deg.)	tanΨ	|cosΔ|	n	k	tanΨ	|cosΔ|	k	n
73	1.54	0.494	1.001	1.502	1.56	0.479	1.029	1.532
74	1.52	0.553	1.000	1.484	1.52	0.530	1.013	1.547
75	1.49	0.604	1.002	1.489	1.49	0.588	1.013	1.534
76	1.46	0.648	1.010	1.505	1.46	0.632	1.007	1.557
77	1.43	0.697	1.010	1.495	1.44	0.674	1.020	1.576
78	1.40	0.734	1.013	1.511	1.41	0.727	1.018	1.552
79	1.38	0.791	1.029	1.452	1.37	0.779	1.022	1.494
80	1.33	0.821	1.003	1.488	1.33	0.817	0.999	1.492
81	1.30	0.861	1.001	1.439	1.29	0.858	0.991	1.464
82	1.26	0.885	1.000	1.482	1.26	0.890	0.998	1.439
Mean			1.007	1.485			1.010	1.519
St. dev.			0.009	0.017			0.013	0.044

Mean of both mirrors: $n' = 1.008$ $k' = 1.494$

Statistical error: $\sigma_n = 0.008$ $\sigma_k = 0.016$

Systematic error: $s_n = 0.020$ $s_k = 0.040$

Table 4: Refractive index at $\lambda_2 = 514.5$ nm and $45^\circ < \theta < 55^\circ$; $\tan\Psi = |\rho_s|/|\rho_p|$.

	Mirror A				Mirror B			
θ (deg.)	$\tan\Psi$	$\lvert\cos\Delta\rvert$	n	k	$\tan\Psi$	$\lvert\cos\Delta\rvert$	k	n
45	1.22	0.802	0.680	1.827	1.21	0.770	0.584	1.695
46	1.23	0.789	0.698	1.854	1.23	0.760	0.633	1.726
47	1.21	0.721	0.553	1.682	1.23	0.751	0.640	1.747
48	1.23	0.729	0.636	1.796	1.24	0.726	0.647	1.766
49	1.22	0.672	0.547	1.696	1.24	0.681	0.588	1.716
50	1.25	0.679	0.645	1.783	1.26	0.677	0.654	1.781
51	1.25	0.614	0.581	1.686	1.26	0.625	0.598	1.714
52	1.26	0.609	0.616	1.759	1.27	0.604	0.622	1.739
53	1.26	0.542	0.567	1.668	1.28	0.562	0.613	1.713
54	1.27	0.525	0.570	1.714	1.27	0.522	0.589	1.708
55	1.29	0.491	0.617	1.710	1.28	0.483	0.590	1.697
Mean			0.612	1.743			0.614	1.728
St. dev.			0.050	0.064			0.026	0.028

Mean of both mirrors: $n' = 0.613$ $k' = 1.733$

Statistical error: $\sigma_n = 0.023$ $\sigma_k = 0.026$

Systematic error: $s_n = 0.010$ $s_k = 0.020$

Table 5: Refractive index at λ_2 = 514.5 nm and $73^\circ < \theta < 82^\circ$; $\tan\Psi = |\rho_s|/|\rho_p|$.

	Mirror A				Mirror B			
θ (deg.)	tanΨ	|cosΔ|	n	k	tanΨ	|cosΔ|	k	n
73	1.27	0.438	0.587	1.683	1.28	0.438	0.598	1.685
74	1.26	0.498	0.585	1.668	1.26	0.486	0.594	1.704
75	1.25	0.550	0.580	1.671	1.26	0.581	0.600	1.710
76	1.24	0.605	0.587	1.665	1.24	0.593	0.604	1.703
77	1.22	0.651	0.584	1.674	1.23	0.644	0.605	1.699
78	1.21	0.701	0.598	1.665	1.22	0.692	0.613	1.703
79	1.19	0.747	0.571	1.660	1.20	0.738	0.601	1.698
80	1.18	0.791	0.585	1.645	1.19	0.784	0.616	1.687
81	1.15	0.826	0.557	1.660	1.15	0.827	0.556	1.654
82	1.14	0.862	0.582	1.655	1.14	0.865	0.552	1.627
Mean			0.582	1.664			0.587	1.687
St. dev.			0.011	0.011			0.022	0.026

Mean of both mirrors: $n' = 0.586$ $k' = 1.671$

Statistical error: $\sigma_n = 0.010$ $\sigma_k = 0.010$

Systematic error: $s_n = 0.020$ $s_k = 0.040$

Figure captions

Fig. 1 : Set-up for the phase-shift Δ_t measurements: P = polarizer prism; FCA1 = air coil 1; M = mirrors' device; FCA2 = air coil 2; FCG = glass Faraday cell; A = analyser prism; D = photodiode.

Fig. 2 : Spectrum of the PSD output taken at the spectrum analyser (Hanning filter) at λ_2 = 514.5 nm; the peak at 3.6 Hz corresponds to the FCA1 rotation, whereas the peak at 4 Hz corresponds to the FCA2 rotation; a): incidence angle $\theta = 78.75^\circ$; b): incidence angle $\overline{\theta}_2 = 78.25^\circ$; here the peak is reduced to the noise level.

Fig. 3 : Set-up for the refractive index measurement: P = polarizer prism; GM = gold mirror; RP = rotating plate; A = analyser prism; D = photodiode; PA = photodiode preamplifier.

Fig. 4 : The dashed lines are obtained by computer calculation using the masured values (11) and (12) of n and k; a): phase shift Δ at λ_2 = 514.5 nm; the corresponding curve at λ_1 = 488 nm is very similar to this one according to tables 2 to 5; b): $\tan\Psi = |\rho_s|/|\rho_p|$.

Fig. 5 : The $|\rho_s|$ and $|\rho_p|$ values of a gold mirror versus the incidence angle θ obtained by computer calculation with the measured values (11) and (12) of n and k.

Fig. 6 : Values obtained for $\overline{Q} = 20 \log Q$ in the configuration of two

reflections around the principal angle $\overline{\theta}_1 = 47.75^\circ$ for $\lambda_2 = 514.5$ nm.

Fig. 7 : Values obtained for $\overline{Q} = 20 \log Q$ in the configuration of two reflections around the principal angle $\overline{\theta}_2 = 78.25^\circ$ for $\lambda_2 = 514.5$ nm.

Fig. 8 : Values obtained for $\overline{Q} = 20 \log Q$ in the configuration of six reflections around the principal angles $\overline{\theta}_1 = 28.25^\circ, \overline{\theta}_2 = 48.25^\circ$, and $\overline{\theta}_3 = 60.5^\circ$ for $\lambda = 514.5$ nm.

Fig. 9 : Spectrum of the PSD output taken at the spectrum analyser (Hanning filter) for $\overline{\theta}_2 = 78.25^\circ$ and $\lambda = 514.5$ nm; the peaks at 144 mHz and 256 mHz correspond to the FCA2 rotation and the peaks at 128 mHz and 272 mHz correspond to the FCA1 rotation signals; the peak at 0.2 Hz corresponds to the second term of eq. (1); a): set-up with the phase-shifter M; the FCA1 signals are reduced to the noise level; b): set-up without the phase-shifter M.

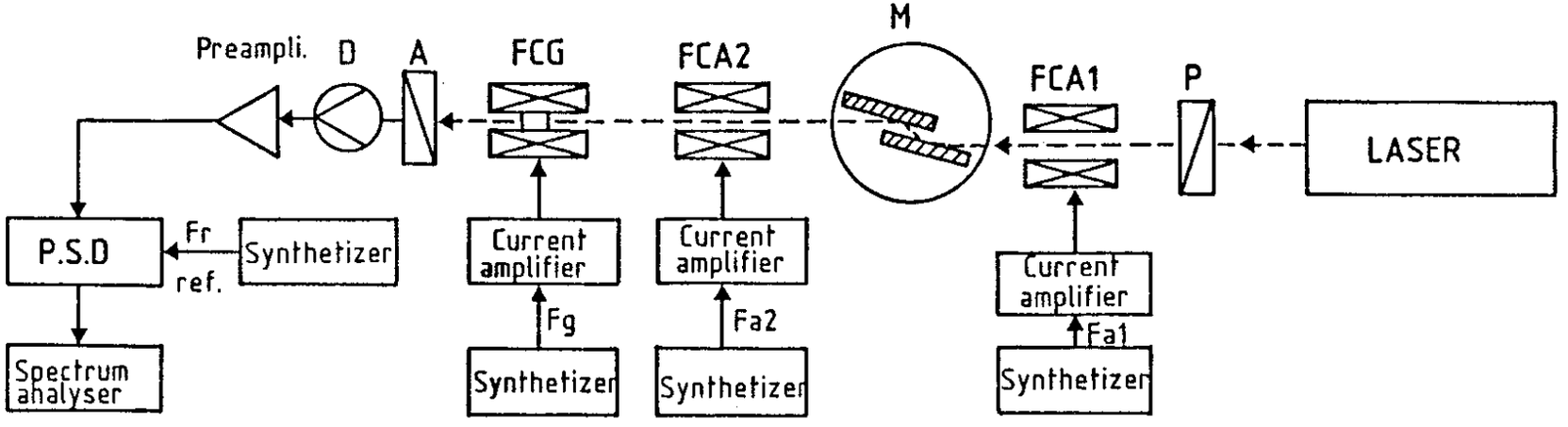
Preampli.
D
A
FCG
FCA2
M
FCA1
P
LASER
P.S.D
Fr
ref.
Synthetizer
Current amplifier
Current amplifier
Current amplifier
Fg
Fa2
Fa1
Spectrum analyser
Synthetizer
Synthetizer
Synthetizer

Fig. 1

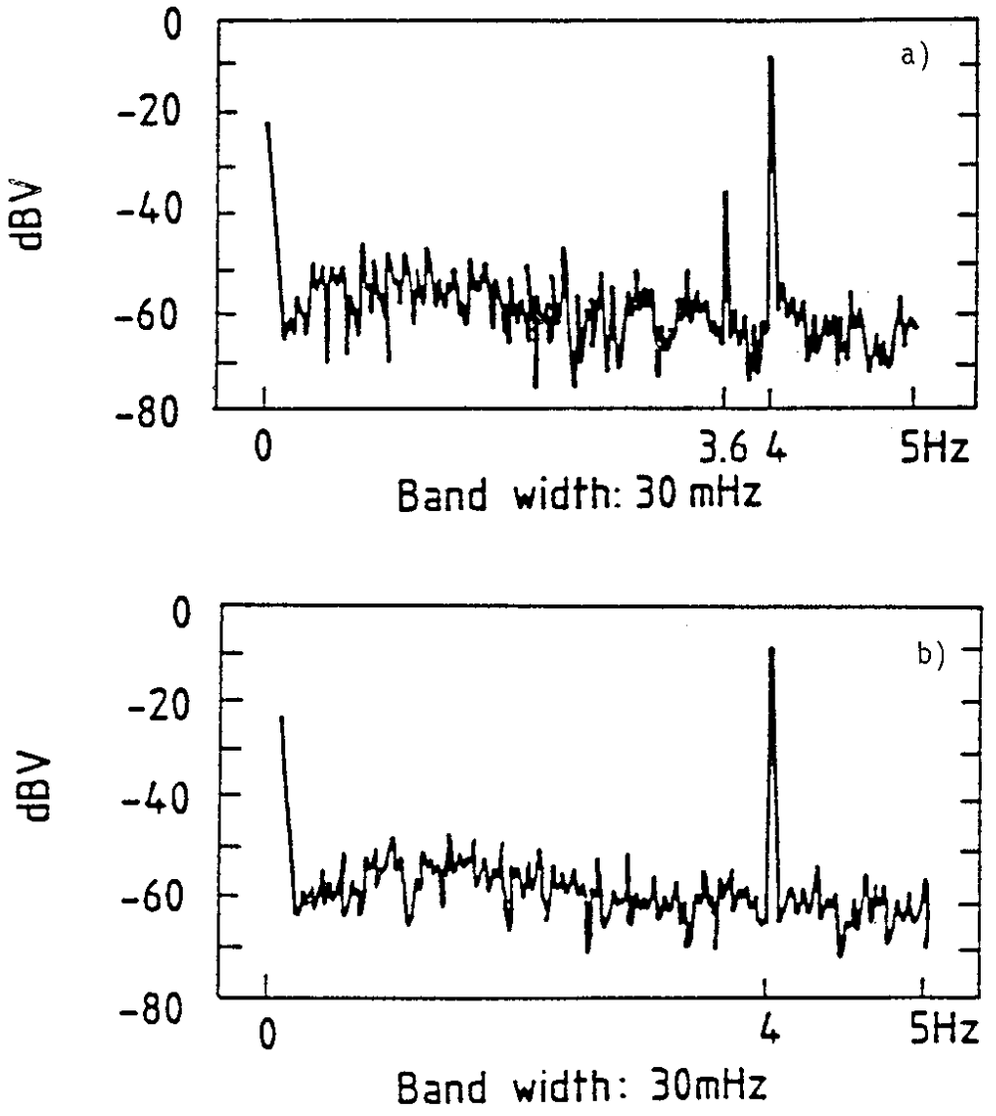
0
-20
-40
-60
-80
dBV
a)
0
3.6 4
5Hz
Band width: 30 mHz
0
-20
-40
-60
-80
dBV
b)
0
4
5Hz
Band width: 30mHz

Fig. 2

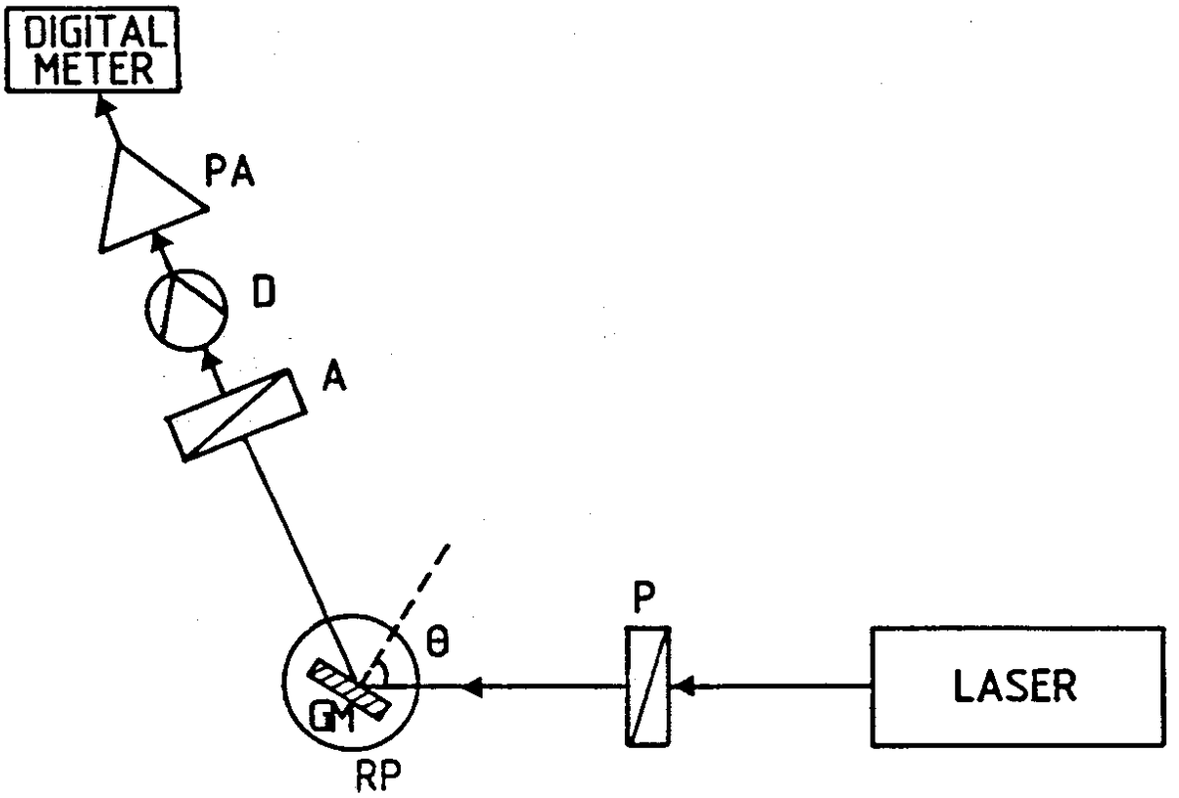

Fig. 3

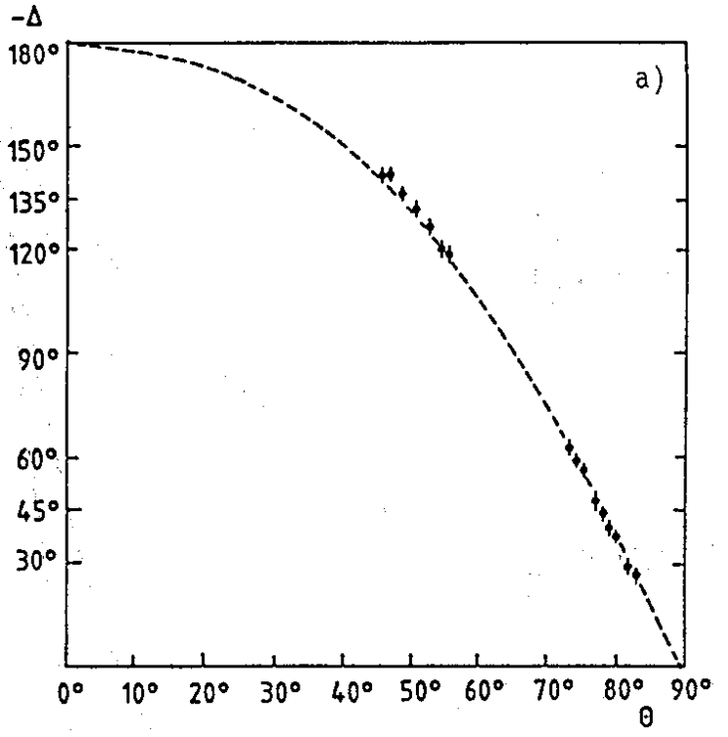
-Δ
180°
150°
135°
120°
90°
60°
45°
30°
a)
0°
10°
20°
30°
40°
50°
60°
70°
80°
90°
θ

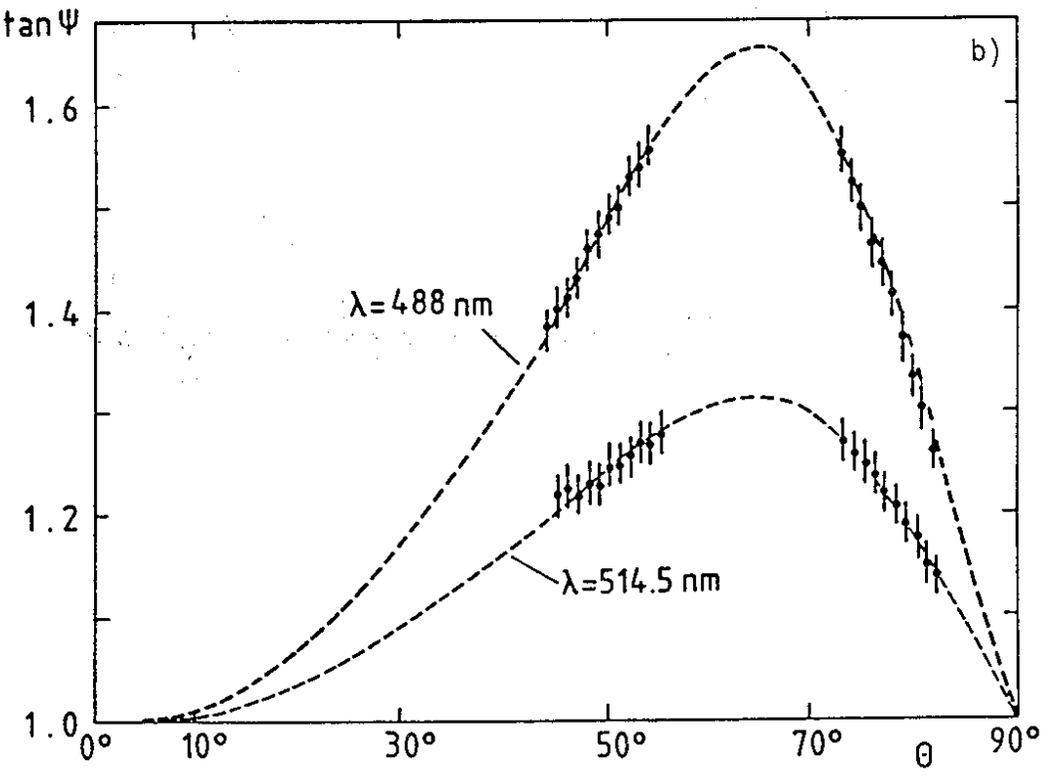
tan Ψ
1.6
1.4
1.2
1.0
b)
λ=488 nm
λ=514.5 nm
0°
10°
30°
50°
70°
90°
θ

Fig. 4

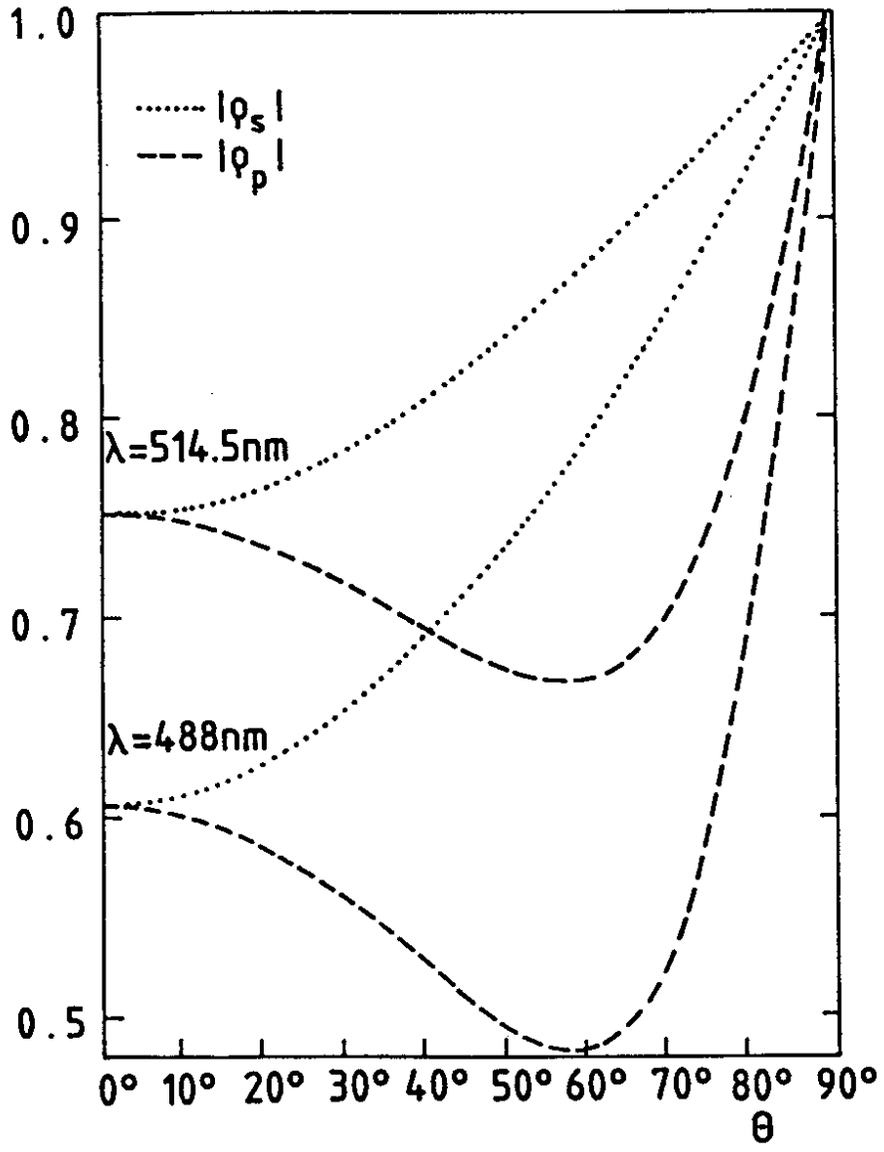
1.0
0.9
0.8
0.7
0.6
0.5
$|\rho_s|$
$|\rho_p|$
λ=514.5nm
λ=488nm
0° 10° 20° 30° 40° 50° 60° 70° 80° 90°
θ

Fig. 5

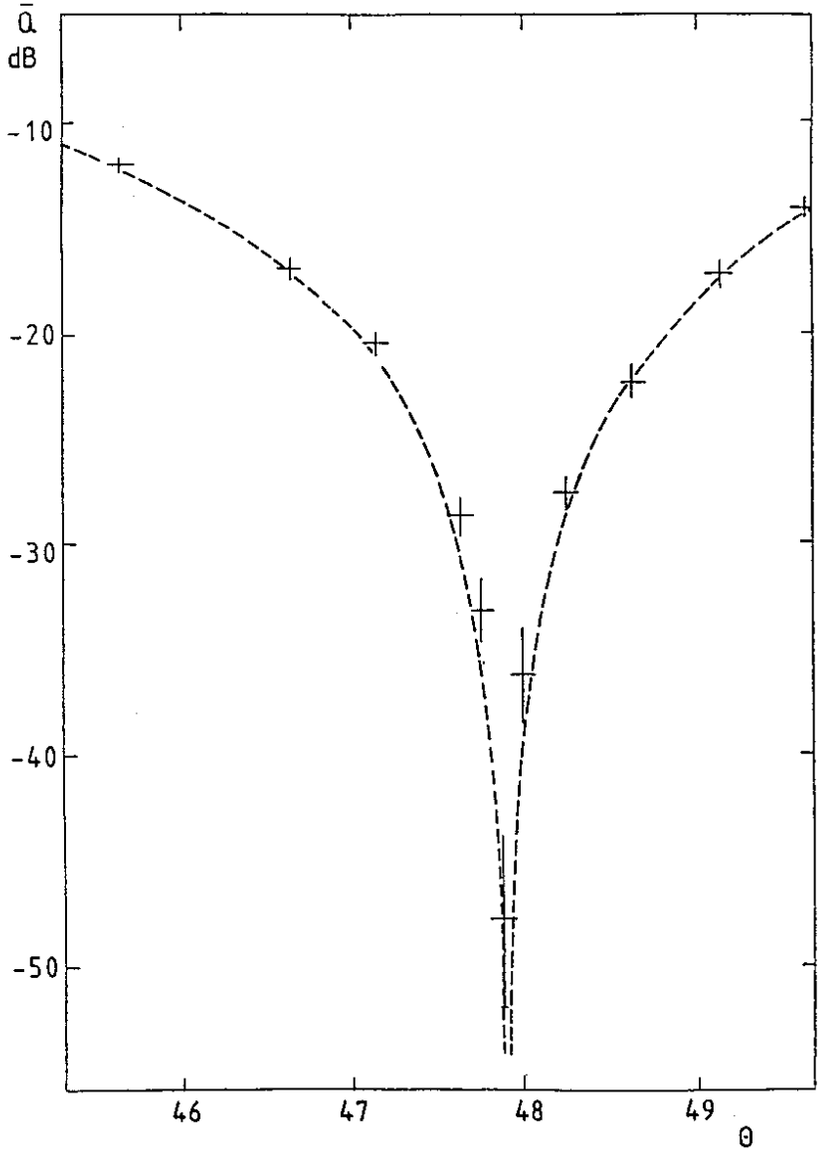
$\bar{Q}$
dB
-10
-20
-30
-40
-50
46
47
48
49
θ

Fig. 6

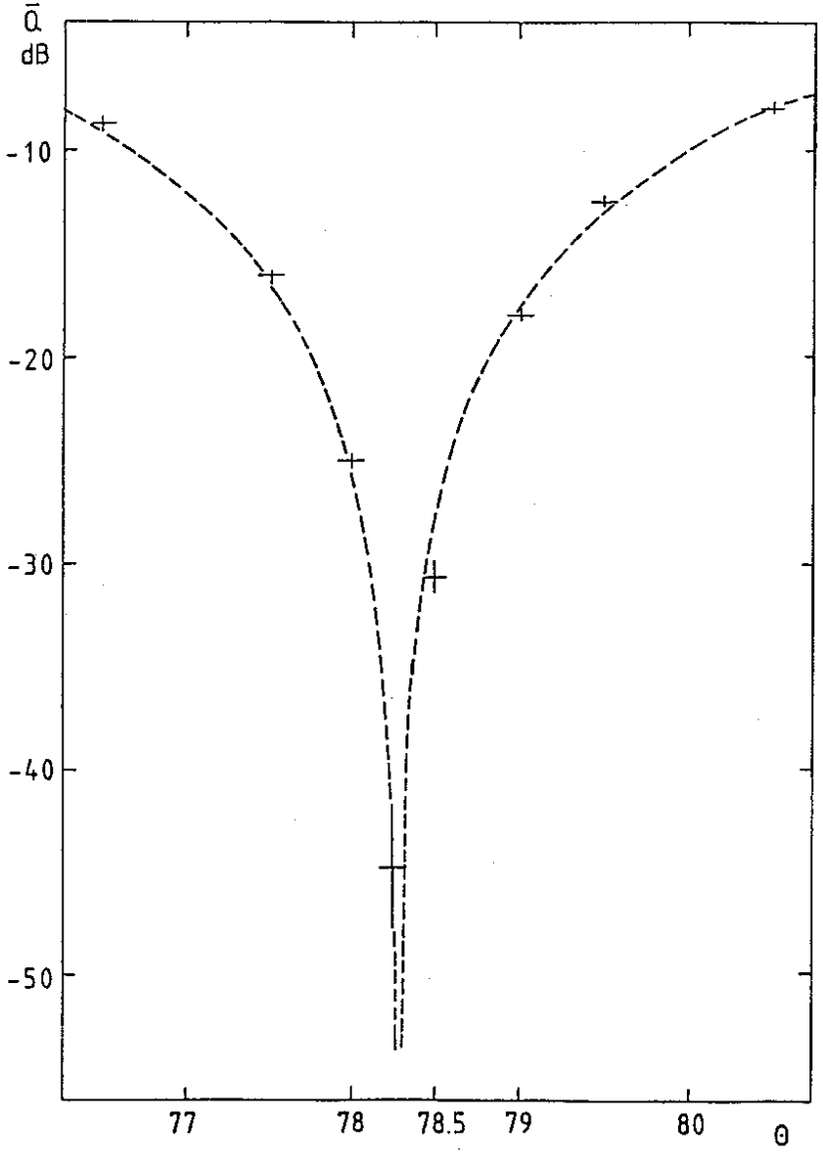
$\bar{Q}$
dB
-10
-20
-30
-40
-50
77
78
78.5
79
80
θ

Fig. 7

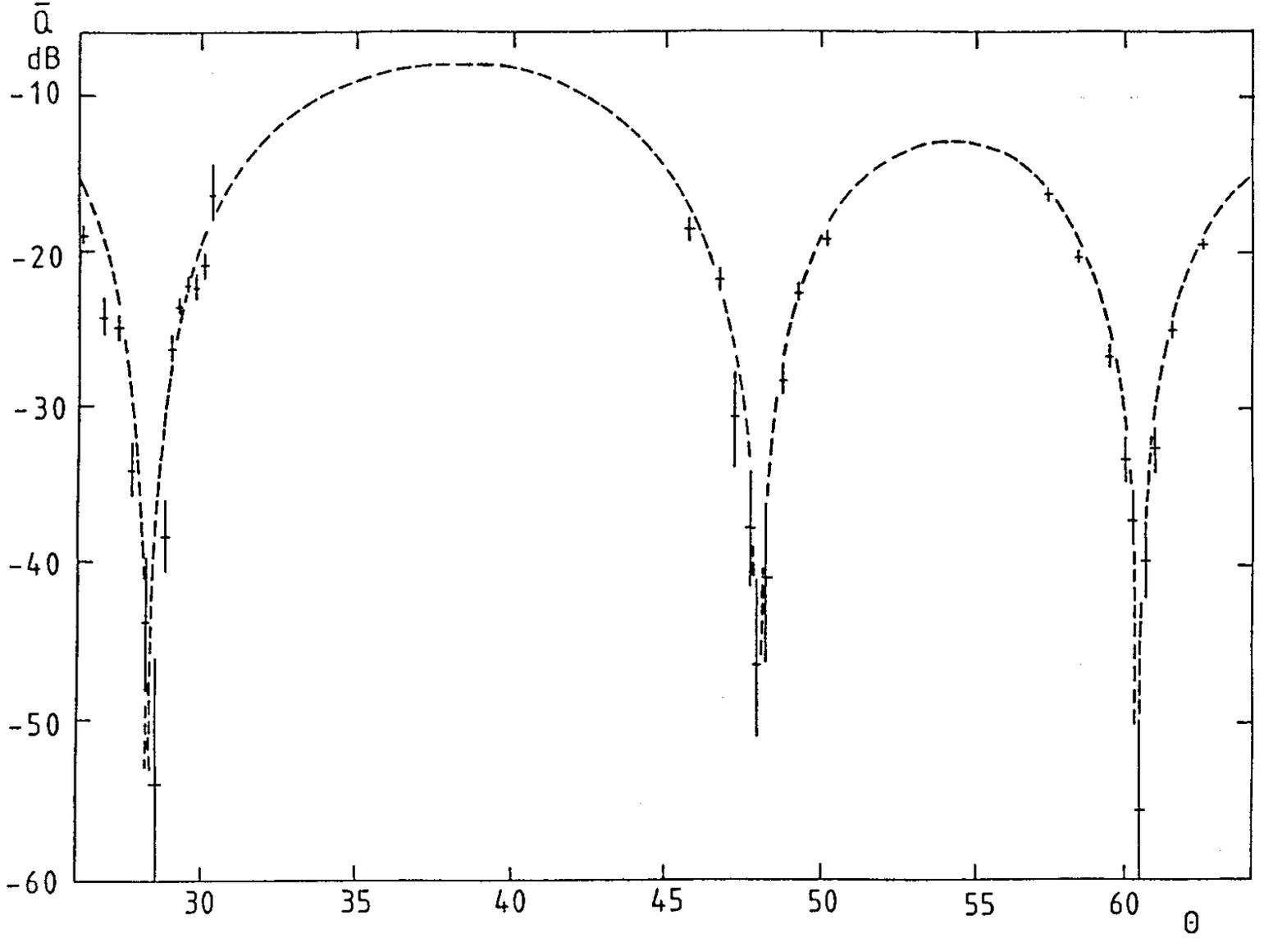

Fig. 8

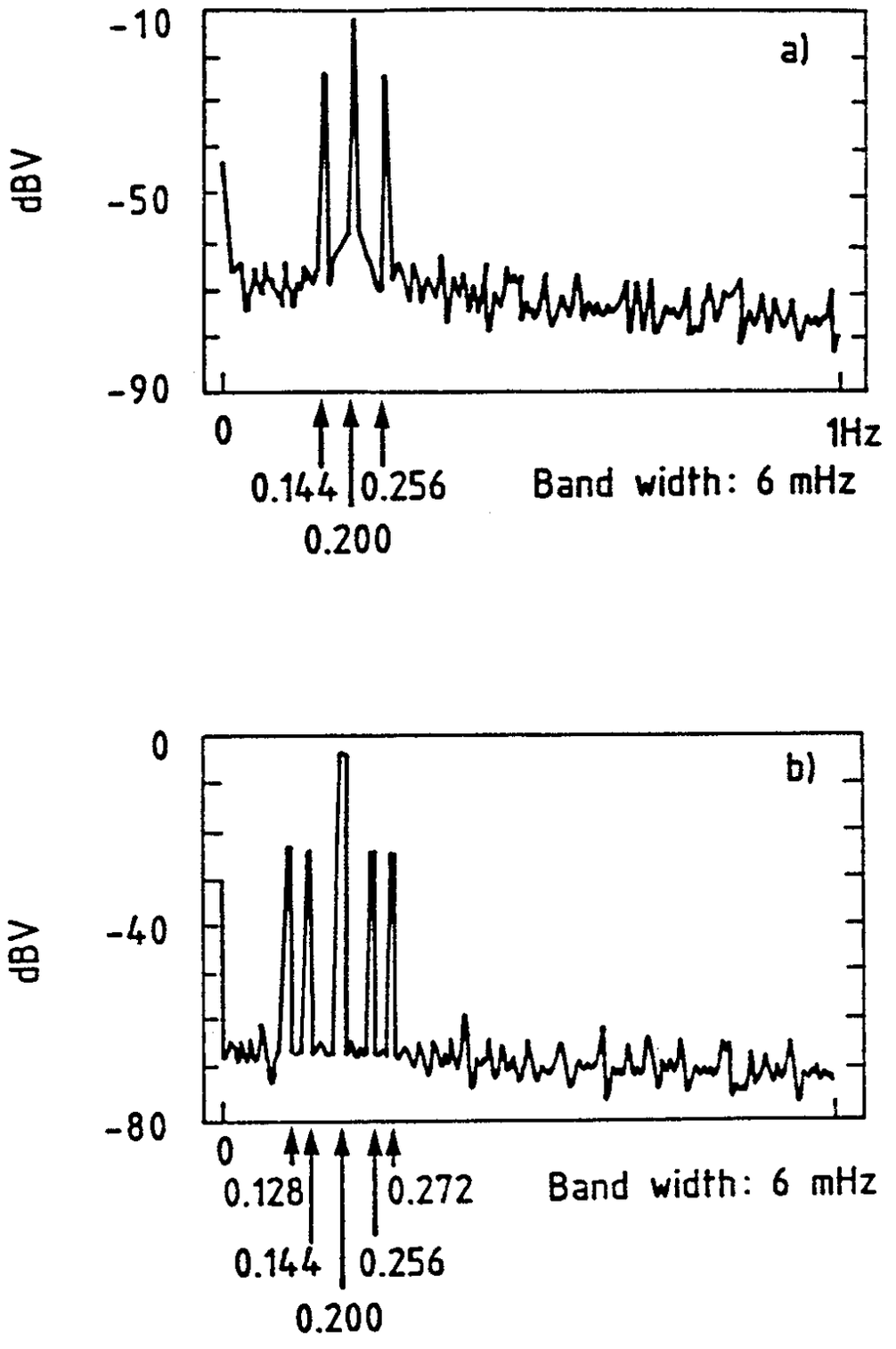
-10
-50
-90
dBV
a)
0
1Hz
0.144
0.256
0.200
Band width: 6 mHz
0
-40
-80
dBV
b)
0
0.128
0.272
0.144
0.256
0.200
Band width: 6 mHz

Fig. 9